Toward Single-Cycle Pulse Generation in Raman-Active Crystals

Miaochan Zhi and Alexei V. Sokolov

(Invited Paper)

***Abstract*—We study broadband sideband generation in Raman-active crystals. The sidebands come out at different angles and cover infrared, visible, and ultraviolet spectral regions. We combine the sidebands into a collinear beam by using a prism. We use a pulse shaper to control the relative phases of the sidebands aiming to produce single-cycle pulses.**

***Index Terms*—Raman crystal, ultrashort pulse generation.**

I. Introduction

SYNTHESIS of ultrashort single-cycle optical pulses requires an over-an-octave-wide coherent spectrum. In the past, broadband collinear Raman generation in molecular gases has been used to produce mutually coherent equidistant frequency sidebands spanning several octaves of optical bandwidths [1]. It has been argued that these sidebands can be used to synthesize optical pulses as short as a fraction of a femtosecond (fs) [2]. The Raman technique relies on adiabatic preparation of near-maximal molecular coherence by driving the molecular transition slightly off resonance so that a single molecular superposition state is excited. Molecular motion, in turn, modulates the driving laser frequencies and a very broad spectrum is generated, hence the term for this process "molecular modulation." By phase locking, a pulse train with a time interval of the inverse of the Raman shift frequency is generated. While at present isolated attosecond X-ray pulses are obtained by high harmonic generation [3], these pulses are difficult to control because of intrinsic problems of x-ray optics. Besides, the conversion efficiency into these pulses is very low (typically 10^{-5}). On the other hand, the Raman technique shows promise for highly efficient production of such ultrashort pulses in the near-visible spectral region, where such pulses inevitably express single-cycle nature and may allow nonsinusoidal field synthesis [2].

Significant recent advances in gas-phase molecular modulation include a demonstration of single-cycle pulse compression [4], and generation of Raman combs with zero offset frequency [5], thereby allowing absolute phase control [6]. In addition, combinations of ns and fs pulses for efficient excitation and probing of molecular coherence in gasses has been explored [7], [8].

We extend the molecular modulation method to Raman-active crystals. The high density of solids leads to high Raman gain. Compared to gas, the higher peak Raman cross-sections in crystals results in a lower stimulating Raman scattering (SRS) threshold, higher Raman gain, and greater Raman conversion efficiency [9]. In addition, there is no need for vacuum systems when working with room temperature crystals, and therefore a compact system can be designed.

Since coherence lifetime in a solid is typically shorter than in a gas, using fs (or possibly ps) pulses is inevitable when working with room-temperature solids. We have studied broadband sideband generation in a Raman-active crystal lead tungstate ($PbWO_4$) either with two 50 fs pulses or a pair of time-delayed chirped pulses [10], [11]. Similar broadband generation is also observed in diamond [12]. Coherent high-order anti-Stokes Raman scattering has also been observed in many other types of crystals such as $YFeO_3$, $KTaO_3$, $KNbO_3$, and TiO_2 when two-color femtosecond (fs) pulses are used [13]–[15]. Progress has been made recently toward synthesis of ultrashort, even few-cycle pulses using Raman crystal. For example, 13 fs pulse generation has been realized in a $KTaO_3$ crystal [16] .

In this paper, we first describe our experimental work on sideband generation in lead tungstate and diamond driven by two- or three-color ultrashort fs pulses or a pair of linearly chirped pulses. We then summarize the characteristics of the sideband generation process in Raman-active crystals. After that, we show our preliminary results on controlling the phases of a subset of the generated sidebands using a pulse shaper; this experiment demonstrates the sidebands' mutual coherence and illustrates our capabilities for precise phase adjustments. This is an important step toward single-cycle pulse generation and nonsinusoidal field synthesis.

II. Broadband Light Generation in Raman Crystals with Two- or Three-Color Laser Fields

A. Experimental Setup

The laser system that we use in this experiment is similar to the one used for femtosecond coherent anti-Stokes Raman scattering (CARS) [17]. The experimental setup is shown in

Manuscript received November 16, 2011; accepted May 26, 2011. Date of publication June 16, 2011; date of current version January 31, 2012. This work was supported in part by the Office of Naval Research, the National Science Foundation (Grant nos. PHY 354897 and 722800), the Texas Advanced Research Program (Grant no. 010366-0001-2007), the Army Research Office (Grant no. W911NF-07-1-0475), and the Robert A. Welch Foundation (Grant no. A1547).

The authors are with the Department of Physics, Institute of Quantum Science and Engineering, Texas A&M University, College Station, TX 77843 USA (e-mail: mczhi@tamu.edu; sokol@physics.tamu.edu).

Color versions of one or more of the figures in this paper are available online at http://ieeexplore.ieee.org.

Digital Object Identifier 10.1109/JSTQE.2011.2159780

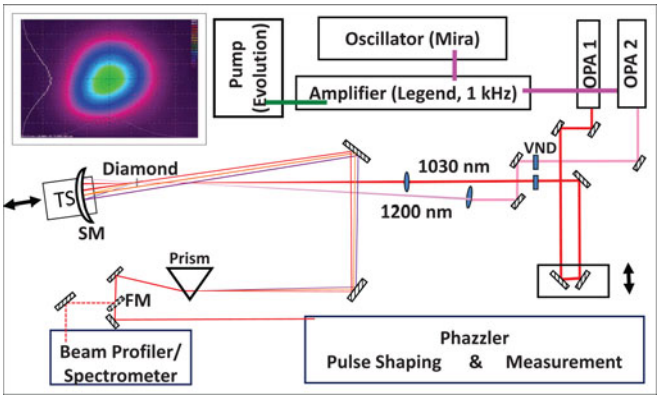

Fig. 1. (a) Schematics of the experimental setup. TS: translation stage, SM: spherical mirror with 10 cm focal length FM: flip mirror, VND: variable neutral density filter. Inset: a beam profile of the combined sidebands which is measured at 1 m after the combining prism.

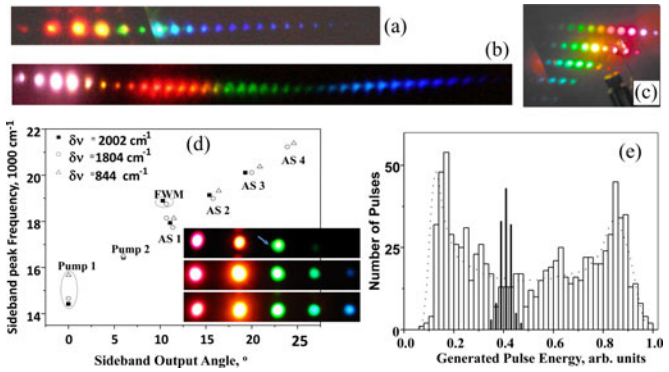

Fig. 2. Raman sidebands generated in $PbWO_4$ with two (a) and three (c) pulses applied to the crystal. Part (b) shows improved generation when a pair of chirped pulses is used. (d) Peak frequency of the generated sidebands [under condition similar to those for (a)] plotted as a function of the output angle; one input frequency is fixed, while the other is tuned; the fact that higher order frequencies remain fixed confirms the Raman-resonant nature of the process. Histogram (e), compared with a theoretical prediction (dotted line) gives a confirmation of the mutual coherence of the generated sidebands. More details can be found in [10].

Fig. 1. We use two computer-controlled optical parametric amplifiers (OPerA, Coherent, with frequency-mixing options), pumped by an amplified femtosecond laser (Mira + Legend, Coherent). The pulses obtained from the two OPAs can be frequency-doubled or mixed with the fundamental pulses to produce up to 30 μJ per 50 fs Gaussian pulses at tunable wavelengths. The pump and Stokes beams are focused and crossed at an angle into the crystal. (Here we use the CARS terminology and call the short wavelength input field as pump beam while the long wavelength one as Stokes beam.) The wavelengths are tuned so that $\nu_{\mathrm{pump}} - \nu_{\mathrm{Stokes}}$ is close to the Raman frequency of the crystal. The angle is chosen such that the CARS phase matching condition for the two peak frequencies of the pump and Stokes beams is satisfied. We put a paper screen after the crystal to take pictures of the sidebands. We combine the sidebands in space and time by means of a spherical mirror and a prism. The inset of Fig. 1 shows a beam profile of the combined sidebands at 1 m after the combining prism.

B. Broadband Light Generation in $PbWO_4$ With Fourier-Transform-Limited Pulses

We first choose lead tungstate ($PbWO_4$), which is a popular crystal for building Raman lasers. It is cheap, nonhygroscopic, and exhibits good optical transparency (from 0.33 to 5 μm). Fig. 2 shows sideband generation in a 1-mm-thick $PbWO_4$ crystal, with two pulses (at 588 nm and 620 nm, with parallel polarizations) applied at an angle of 4° (parts a, d, and e), and three pulses applied for part (c). We observe up to 20 anti-Stokes (AS) and 2 Stokes (S) sidebands projected on a white screen, as shown in Fig. 2(a), with the pump beams and the first 3 AS beams being attenuated by a neutral density filter. When we measure the spectrum of the anti-Stokes sidebands, we observe several interesting features: the spectra of the lower-order sidebands show a rich structure, possibly due to simultaneous excitation of several Raman lines (in $PbWO_4$, there are strong Raman transitions at 901 cm^{-1} and 323 cm^{-1}). The spectra of the high-order sidebands are cleaner. The picture shows all sidebands equally spaced on the screen (spatially separated by equal angles), but with a (barely-noticeable) cusp (around AS 4) in the line that can be drawn through the spots. In addition, we demonstrate that we can use three input pulses to obtain a 2-D array of beams of varying colors [Fig. 2(c)]. The three beams are focused into the crystal with a typical BoxCARS geometry (see [18]). For example, we use pulses at 804 nm, 730 nm, and 604 nm to generate up to 50 beams of different colors.

In contrast to the experiment in the molecular gas, where the sidebands have equal frequency separations between adjacent orders, the frequency separations of the sidebands which are generated in the crystal are decreasing gradually from 900 cm^{-1} down to 450 cm^{-1} as the sideband order goes higher. One may wonder whether the sidebands are generated by a Raman process and whether there is mutual coherence among the sidebands. To prove the Raman-resonant nature of sideband generation, and to separate the effect of instantaneous four wave mixing (FWM), we tune the difference between the two applied laser frequencies and measure the generated AS frequencies as a function of the angle, as shown in Fig. 2(d). We find that the generated AS 1 beam splits into two slightly separated distinctively colored beams: one corresponding to (nonresonant) FWM and the other (which is much brighter) corresponding to Raman-resonant AS generation. We observe that as we vary the frequency separation between the two pump beams from 844 to 2002 cm^{-1} the Raman sidebands are generated at approximately the same angle and with roughly the same frequency shift from the previous order.

Next, we investigate the mutual coherence among the generated sidebands. We first generate multiple AS sidebands by focusing two beams (Red and IR) into the $PbWO_4$ crystal. Then a third (yellow) beam is sent along the direction of the generated AS 3 sideband with a matching wavelength to that of AS 3. We measure the pulse energy of AS 5 on a shot-by-shot basis by using a fast photodiode once overlap in frequency, space, and time is achieved. The statistics of the AS 5 pulse energy is shown in Fig. 2(e). Solid black bars give the histogram (number of pulses

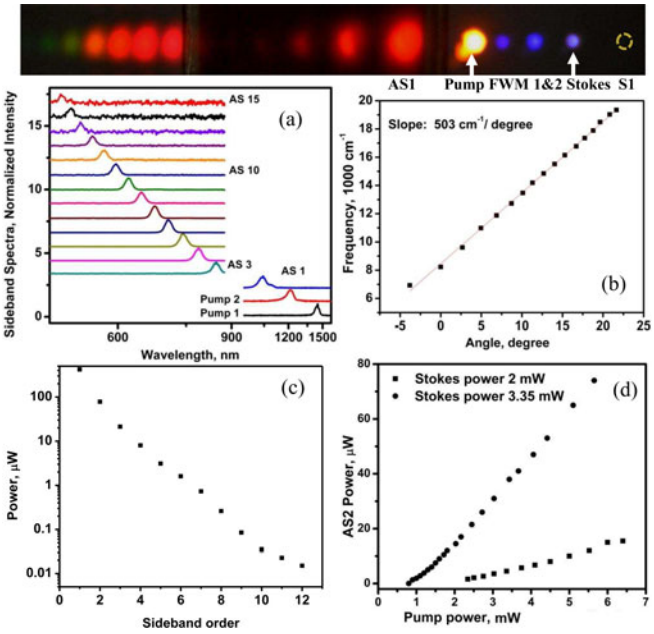

Fig. 3. Spectral sideband generation in CVD single-crystal diamond. Top: The generated beams are projected onto white paper 30 cm away from the crystal. A near-IR viewing card is used to show the AS 2 to AS 6. FWM 1 & 2 signals have frequency of $2\omega_{\rm pump} + \omega_{\rm Stokes}$ and $2\omega_{\rm Stokes} + \omega_{\rm pump}$, respectively. (a) The spectra of the two pump beams and the generated sidebands. Reciprocal scale is used for the x-axis. (b) The peak frequency of the pump, Stokes, and the generated sidebands versus the external output angle. (c) The power of the sidebands. Log scale is used for the vertical axis. (d) The power dependence of the AS 2 as a function of the pump beam power at two different levels of Stokes power; for (d) the pump and Stokes wavelengths are 1055 nm and 1230 nm, while for all other parts they are 1215 nm and 1440 nm.

versus AS 5 energy), with only Red and IR pulses applied at the input. This histogram shows a typical normal distribution, with about 10% average variations. However, with the addition of the Yellow beam at the input, the histogram of the AS 5 pulse energy (913 pulses total) transforms into a very different distribution (Fig. 3, white bars). We perform a simple calculation which agrees well with the experimental result and confirms that the sidebands are mutually coherent [10].

C. Broadband Light Generation in Synthetic Diamond

Coherent multiple-order sideband generation in the femtosecond regime is not limited to $PbWO_4$, but can be obtained in other solids. For example, diamond's unique optical properties, in particular the largest transparency range (from far infrared to ultraviolet), and high damage threshold, combined with a strong Raman activity (dominant mode at 1332 cm^{-1}, with a linewidth of 3.3 cm^{-1}, corresponding to a 3.2 ps dephasing time) all make diamond a unique candidate for experiments on broadband Raman generation. Diamond's other important properties include the highest atom-number density and the highest thermal conductivity of any solid. Recently, optical-quality synthetic diamond plates [obtained by the chemical vapor deposition (CVD) technique] have become available, for a reasonable price. We note that a highly efficient Raman laser has been built using diamond recently [19].

With diamond, we have obtained qualitatively similar results (as with $PbWO_4$), with the main quantitative differences possibly coming from the fact that the Raman spectrum of diamond is less complicated and diamond is isotropic. The fact that diamond has a broader transmission window and correspondingly smaller dispersion may also have contributed to the differences. Nonlinear frequency conversion in diamond is very efficient (similar to $PbWO_4$); for example, in one experiment we have measured 7% conversion efficiency into the first anti-Stokes sideband and 1% into the second anti-Stokes and first Stokes.

Sideband generation in diamond are summarized in Fig. 3. The center wavelengths of the pump and Stokes pulses are at 1215 and 1440 nm, respectively [except for part (d), where the input wavelengths used were 1055 nm and 1230 nm]. The diamond crystal is about 1.0 mm thick. We measure 15 AS sidebands (Fig. 3 top). The Stokes beam appears blue because third harmonic generation occurs in the crystal and superimposes with the IR beam. The two blue-color beams in between the pump and Stokes beams are two FWM signals from the pump and Stokes beams. They have frequency of $2\omega_{\rm pump} + \omega_{\rm Stokes}$ and $2\omega_{\rm Stokes} + \omega_{\rm pump}$, respectively. The dotted circle shows the position of the first Stokes beam, which can only be seen through an IR viewer. The spectra of the sidebands are shown in Fig. 3(a) while in (b) we show the peak frequency of the sidebands as a function of angle. The power of each sideband is given in Fig. 3(c). The power is decreasing approximately exponentially. Fig. 3(d) shows how the AS 2 (less affected by FWM) power varies with the pump beam power for two different Stokes beam power levels. We find that at low power it is a higher-order power law. The dependence soon changes to linear as we increase the power. We can see that high pump beam power is desirable. However, limited by parasitic nonlinear processes, such as self phase modulation (SPM) and white light generation, only less than 5 mW pump power can be used when we focus the beam with a 50 cm focal length lens. Next we show that more pump power can be applied if chirped pulses are used.

D. Broadband Generation in $PbWO_4$ With a Pair of Linearly Chirped Pulses

To scale up the power and to improve the efficiency of this experiment, we excited the $PbWO_4$ crystal with two linearly chirped pulses. Temporal stretching of the excitation pulses allows us to use large pulse energies per unit area (while still avoiding parasitic nonlinear effects), and correspondingly increase the Raman coherence. In order to optimize the generation process we study the effect of time delay (or the pulse chirp rate), and the crossing angle between the two pump beams, on the efficiency of sideband generation. We measure up to 40 AS and 5 S sidebands generated when a Raman mode at 190 cm^{-1} is resonantly excited. In this case, the conversion efficiency from the two pump beams into the sidebands is high; for example, we have measured as high as 41% conversion efficiency for the pump beam and 21% for the Stokes beam. Compared to the fs excitation, we observe more sidebands generated by the chirped pulses (the AS sidebands cover a range of 12 000 cm^{-1} wide).

Although the FWM process still creates some multiple peaks in the spectra of the low-order sidebands, the complications due to simultaneous excitation of multiple Raman lines are eliminated. Different Raman modes can be selectively excited by varying the time delay and the angle between the two pump beams. Our experiment confirms that phase matching plays an important role in the Raman generation process.

III. Characteristics of Broadband Light Generation in Raman Crystals with Two-Color FS Laser Fields

We find that the broadband light generation in Raman crystals shares the following common features:

1) Phase matching is critical: In general, due to the large dispersion in solids, a noncollinear beam geometry is needed for efficient excitation in a Raman crystal. In SRS and in Raman lasers, high conversion efficiency is often achieved by using a much thicker sample or an external cavity. For example, when $PbWO_4$ is used in a Raman laser, a typical thickness is up to 70 mm [20]. As a comparison, the sample we use is 1 mm thick. Therefore the linear dispersion and competing nonlinear optical effects such as SPM are minimized. However, compared to the experiment with low pressure gas, phase matching plays an important role. The use of a nonzero angle is critical; for collinear beams we observe week generation of only lowest-order sidebands. When the beams cross at angles between 2 and 8 degrees, we observe efficient nonlinear generation of many spatially well-separated sidebands. Correspondingly, due to the material dispersion, phasematching is optimized when sidebands of different colors propagate at different angles. We have seen a sideband come out at almost 80^o with respect to the pump beam. The intensity may not be monotonously decreasing as the order goes higher due to the large phase mismatch for certain sidebands [11].
2) Resonance requirement is relaxed: The requirement of the frequency spacing between the two pump pulses to be tuned to Raman frequency is greatly relaxed since we are using fs pulses which have about 450 cm^{-1} bandwidth (FWHM). Moreover, the broad Raman spectral linewidth (compared to gas medium) also eases the resonance requirement. We have observed Raman generation in diamond even when we tuned the $\nu_{\rm pump} - \nu_{\rm Stokes}$ to double the Raman frequency. One more proof is that we have observed the simultaneous excitation of 325 cm^{-1} and 901 cm^{-1}, which leads to quantum beating in signal [21].
3) SPM is suppressed when Raman sidebands are generated: As mentioned earlier, large pump power leads to high sidebands power. However, we are limited by the SPM, so only a few mW power can be used. We normally start with the beam energy right below the SPM threshold. After we find the overlap and observe generation, we can increase the two pump beams power further without causing SPM. In a way, we can say that the Raman generation process suppresses the SPM process. A similar situation has been observed in the gas experiment using fs pulses [22].

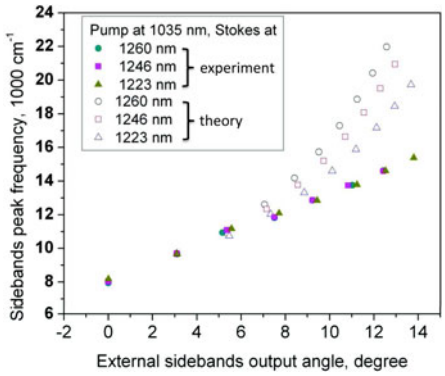

Fig. 4. The measured peak frequency of the pump, Stokes, and the generated sidebands versus the external output beam angle at three different pump wavelengths (solid symbols: circle, square, and triangle). The open symbols show sideband frequencies which are calculated by using the method described in [23], where they assume a cascading FWM process.

4) Both processes—the (Raman nonresonant) instantaneous FWM process and the Raman process—often coexist: However, we believe the (higher-order) sidebands are generated through the Raman process, as described in Section II-B and shown in Fig. 2(d). The FWM signals (fewer, typically 2 to 3 orders) superimpose on the Raman sidebands or locate in between the sidebands. As a result, the spectral shapes of these lower-order sidebands sometimes show complex spectral shapes with multiple peaks.
   This can be further proved by the following: We have performed a theoretical calculation assuming a nonresonant cascading FWM process, following the method described in detail by Liu *et al.*, which works well for calculating the cascading FWM signals generated in fused silica or BBO [23]–[25]. The result is shown in Fig. 4. We can see that as we tune the Stokes wavelength, the sidebands' central frequency predicted by the theoretical calculation changes dramatically, especially for higher orders. However, our experimental results show much less variation.

   In addition, we notice that although the measured frequency spacing of the sidebands decreases at higher AS orders, it is linear as a function of the external output angle [Fig. 3(b)]. This seems to be only true if the generation is dominated by the Raman process, and not by the cascading FWM process.
5) There are more AS sidebands produced than S sidebands: In these experiments, we observe a larger number of AS sidebands than Stokes ones. This asymmetry is typically present since the Raman frequency is only one or two orders of magnitude smaller than the laser frequency, and hence the total generated bandwidth is comparable to the pump laser frequency. At substantially lower frequencies generation is intrinsically less efficient. In addition, infrared sidebands are harder to detect. Finally, in the present experiment phase matching occurs at a considerably larger output angle (and leads to a correspondingly worse

spatial overlap with the pump beams) for a Stokes sideband compared to the same order AS sideband.

6) There are differences between the sideband generation processes due to excitation of large- and small-frequency Raman modes: The sideband generation due to excitation of large- and small-frequency Raman modes shows few distinct differences. In the case of a large-frequency Raman mode, a large angle is needed to fulfill the phase-matching condition. As a result, the deviation of the frequency spacing from the Raman frequency is getting large as the sideband order goes higher. For broadband generation with 325 cm^{-1} or even lower Raman frequency of 191 cm^{-1}, almost constant frequency spacing can be maintained up to a very high order, and therefore, more than 40 sidebands can be generated.
7) The generated sidebands have good beam quality (Fig. 1 inset) and have similar pulse duration to those of the pump pulses. This is similar to the sidebands generated through cascading FWM process [25].

IV. Single-Cycle Pulse Synthesis by Pulse Shaping

The dispersion in the solids not only requires noncollinear pumping geometry, but also produces sidebands coming out at almost regularly spaced angles. As mentioned earlier, although the frequency spacing of the sidebands is different, it is linear as a function of the external output angle. This linearity enable us to combine the sidebands in space and time by using a spherical mirror and a prism (as per Fig. 1; also see [16]). In this experiment, we use a 1-mm-thick CVD single-crystal diamond. The pump pulse is centered at 1030 nm while the Stokes pulse is at 1200 nm. The center wavelength of AS 1, 2, 3 sidebands is 910 nm, 830 nm, and 770 nm, respectively. We first measure the slope of peak frequency of the sidebands versus angle. Then we carefully adjust the distance from the crystal to the spherical mirror, the distance from spherical mirror to the prism, and the angle of the prism to match the spreading angle of the sidebands. A single combined beam can be obtained this way. The distance from the crystal to the spherical mirror is about 11 cm; the prism is about 1.6 m away from the spherical mirror. We use the tip of the prism to minimize the dispersion. The beam is incident on the prism at the minimum deviation angle. The combined beam is diagnosed with a beam profiler located 1 m after the prism. After that, it is sent to an acousto-optic pulse shaper (Phazzler, FastLite), which has the capability of both pulse measurement and pulse shaping. Specifically, there is a thin BBO crystal after the Dazzler, the pulse shaping unit, which enables collinear second harmonic generation (SHG) frequency resolved optical gating (FROG) measurement of pulses with pulse duration down to 20 fs [26].

Diagnostics and optimization of relative phases of sidebands which have spectrally well-separated peaks are not trivial [27]. Retrieval of a directly measured SHG FROG trace may not converge and, therefore, may not give reasonable pulse duration and phase information. As has been pointed out by Hänsch more than 20 years ago, in order to compare the phases of waves with different frequencies, a nonlinear process such as sum frequency generation (SFG) must be employed [28]. Here we use SFG between the sidebands to adjust the relative phase of the sidebands in pairs, which is similar to the method used by Kung *et al*. [29].

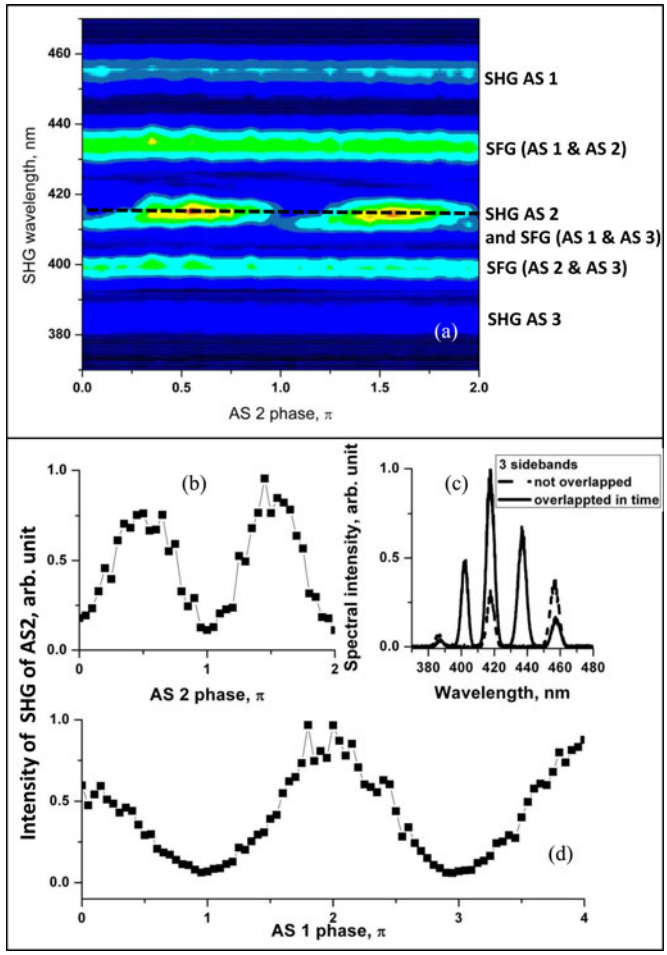

Fig. 5. (a) SHG spectra of the first three sidebands as we vary the AS 2 phase from 0 to 2π. (b) The peak intensity at the SHG of AS 2 peak [along the dotted line in (a)] as a function of the AS 2 phase, with AS 1 and AS 3 phase fixed. (c) SHG spectra of the three sidebands when they are not overlapped (dashed line) and overlapped (solid line) in time. (d) The peak intensity of the SHG of AS 2 region as a function of the AS 1 phase, with AS 2 and AS 3 phases fixed.

Preliminary data with three sidebands are shown in Fig. 5. The SHG of the first three sidebands is shown in Fig. 5(c). The dashed line shows the case when the three sidebands are not overlapped in time. The solid line shows the result when the three pulses overlapped in time after we adjust the timing between the pulses by using the pulse shaper. Strong SFG between the sidebands is seen. Also, SFG between AS 1 and AS 3 overlaps, both in time and spectrum, with SHG of AS 2. When we vary the phase of AS 2 [centered around 415 nm in Fig. 5(b)] from 0 to 2π and record the peak intensity at the SHG of AS 2 region, we observe a sinusoidal change of the intensity, as a result of the beating between SHG of AS2 and SFG of AS 1 and AS 3. When we vary the phase of AS 1 and again record the peak intensity of the same signal peak [Fig. 5(d)], we observe a similar dependence, only with half the period [Fig. 5(b)]. This is as expected since the peak intensity of SHG of AS 2 is a function of $\cos(2\varphi_2 - \varphi_1 - \varphi_3)$,

where φ_1, φ_2, and φ_3 are the spectral phases of each sideband, respectively. We also record the peak intensity of the spectrum at the SHG of AS 2 region as a function of AS 3 phase. The result has a similar beating as the one when scanning AS 1 phase. These experiments demonstrate the mutual coherence of the spectral sidebands, and show the pulse shaper's capability to control their phases in a precise and stable manner [30].

When the phases across the three sidebands' spectra are adjusted to all be equal, the resultant pulse duration is expected to be 11 fs (FWHM). If five sidebands are included, we expect to generate pulses with 5.6 fs pulse duration. Our limitation so far is set by the pulse shaper which operates at wavelengths range from 530 nm to 930 nm, so at most six sidebands can be used for pulse shaping; utilization of this full bandwidth will enable us to produce pulses as short as 4.8 fs. Significant advances beyond that point can be obtained when two (or more) pulse shapers covering adjacent spectral ranges are used.

V. Conclusion and Future Work

We realize broadband light generation in Raman-active crystals using the molecular modulation method. We experimentally study the characteristics of the generation process in two types of crystals—lead tungstate and diamond. We show preliminary result of controlling the relative phases of three sidebands.

In the future, we will extend this phase adjustment to more sidebands. After that, we plan to not only adjust the phase, but also the amplitude of the sidebands to produce arbitrary waveforms. We note that the broadband light generation in crystals has substantial room for improvement by refining the setup and applying the pulse shaping technique not only to the generated sidebands but also to the two pump beams. We also want to address whether it is possible to realize collinear generation of sidebands in Raman crystals driven by a pair of linearly chirped pulses. First of all, this setup would allow pulse shaping without the combining optics; second, more power can be used, as described in Section 2.4. Finally, we want to carry out a rigorous numerical simulation of sideband generation, including the production of the 2-D color arrays [Fig. 1(b)]. This simulation may provide a better understanding of the generation process and, thus, enable further optimization of the sideband generation process.

Acknowledgment

The authors thank their friend Jun Liu who generously shared his code with them.

References

[1] A. V. Sokolov and S. E. Harris, "Ultrashort pulse generation by molecular modulation," *J. Opt. B: Quantum Semiclassical Opt*., vol. 5, pp. R1—-R26, 2003.

[2] A. V. Sokolov, M. Y. Shverdin, D. R. Walker, D. D. Yavuz, A. M. Burzo, G. Y. Yin, and S. E. Harris, "Generation and control of femtosecond pulses by molecular modulation," *J. Modern Opt*., vol. 52, pp. 285–304, 2005.

[3] P. B. Corkum and F. Krausz, "Attosecond Science," *Nature Phys*., vol. 3, pp. 381–387, 2007.

[4] M. Y. Shverdin, D. R. Walker, D. D. Yavuz, G. Y. Yin, and S. E. Harris, "Generation of a single-cycle optical pulse," *Phys. Rev. Lett*., vol. 94, no. 3, p. 033904, 2005.

[5] T. Suzuki, M. Hirai, and M. Katsuragawa, "Octave-Spanning Raman Comb with Carrier Envelope Offset Control," *Phys. Rev. Lett*., vol. 101, pp. 243602-1–243602-4, 2008.

[6] Z. Hsieh, C. Lai, H. Chan, S. Wu, C. Lee, W. Chen, C. Pan, F. Yee1, and A. H. Kung, "Controlling the Carrier-Envelope Phase of Raman-Generated Periodic Waveforms," *Phys. Rev. Lett*., vol. 102, p. 213902, 2009.

[7] N. Zhavoronkov and G. Korn, "Generation of Single Intense Short Optical Pulses by Ultrafast Molecular Phase Modulation," *Phys. Rev. Lett*., vol. 88, no. 20, p. 203901, 2002.

[8] S. Gundry, M. P. Anscombe, A. M. Abdulla, E. Sali, J. W. G. Tisch, P. Kinsler, G. H. C. New, and J. P. Marangos, "ltrashort-pulse modulation in adiabatically prepared Raman media," *Opt. Lett*., vol. 30, pp. 180–182, 2005.

[9] T. T. Basiev and R. C. Powell, "Introduction," *Opt. Mater*., vol. 11, pp. 301–306, 1999.

[10] M. Zhi and A. V. Sokolov, "Broadband coherent light generation in a Raman-active crystal driven by two-color femtosecond laser pulses," *Opt. Lett*., vol. 32, pp. 2251–2253, 2007.

[11] M. Zhi and A. V. Sokolov, "Broadband generation in a Raman crystal driven by a pair of time-delayed linearly chirped pulses," *New J. Phys*., vol. 10, p. 025032, 2008.

[12] M. Zhi, X. Wang, and A. V. Sokolov, "Broadband coherent light generation in diamond driven by femtosecond pulses," *Opt. Exp*., vol. 16, pp. 12139–12147, 2008.

[13] J. Takahashi, "Generatoin of a broadband spectral comb with multiwave mixing by exchange of an impulsively stimulated phonon," *Opt. Exp*., vol. 12, pp. 1185–1191, 2004.

[14] E. Matsubabra, K. Inoue, and E. Hanamura, "Dynamical symmetry breaking induced by ultrashort laser pulses in $KTaO_3$," *J. Phys. Soc. Jpn*., vol. 75, p. 024712, 2006.

[15] H. Matsuki, K. Inoue, and E. Hanamura, "Multiple coherent anti-Stokes Raman scattering due to phonon grating in $KNbO_3$ induced by crossed beams of two-color femtosecond pulses," *Phys. Rev. B*, vol. 75, p. 024102, 2007.

[16] E. Matsubara, Y. Kawamoto, T. Sekikawa, and M. Yamashita, "Generation of ultrashort optical pulses in the 10 fs regime using multicolor Raman sidebands in $KTaO_3$," *Opt. Lett*., vol. 34, pp. 1837–1839, 2009.

[17] D. Pestov, R. K. Murawski, G. O. Ariunbold, X. Wang, M. Zhi, A. V. Sokolov, V. A. Sautenkov, Y. V. Rostovtsev, A. Dogariu, Y. Huang, and M. O. Scully, "Optimizing the laser-pulse configuration or coherent Raman spectroscopy," *Science*, vol. 316, p. 265, 2007.

[18] D. Pestov, M. Zhi, Z. Sariyanni, N. G. Kalugin, A. A. Kolomenskii, R. Murawski, G. G. Paulus, V. A. Sautenkov, H. Schuessler, A. V. Sokolov, G. R. Welch, Y. V. Rostovtsev, T. Siebert, D. A. Akimov, S. Graefe, W. Kiefer, and M. O. Scully, "Visible and UV coherent Raman spectroscopy of dipicolinic acid," *Proc. Nat. Acad. Sci*., vol. 102, pp. 14976–14981, 2005.

[19] R. P. Mildren and A. Sabella, "Highly efficient diamond Raman laser," *Opt. Lett*., vol. 34, pp. 2811–2813, 2009.

[20] A. A. Kaminskii, C. L. McCray, H. R. Lee, S. W. Lee, D. A. Temple, T. H. Chyba, W. D. Marsh, J. C. Barnes, A. N. Annanenkov, V. D. Legun, H. J. Eichler, G. M. A. Gad, and K. Ueda, "High efficiency nanosecond Raman lasers based on tetragonal $PbWO_4$ crystals," *Opt. Commun*., vol. 183, pp. 277–287, 2000.

[21] M. Zhi, X. Wang, and A. V. Sokolov, "Broadband light generation using a relatively weak Raman mode in lead tungstate crystal," *J. Modern Opt*., vol. 57, no. 19, pp. 1863–1866, 2010.

[22] E. Sali, K. J. Mendham, J. W. G. Tisch, T. Halfmann, and J. P. Marangos, "High-order stimulated Raman scattering in a highly transient regime driven by a pair of ultrashort pulses," *Opt. Lett*., vol. 29, pp. 495–497, 2004.

[23] R. Weigand, J. T. Mendonca, and H. M. Crespo, "Cascaded nondegenerate four-wave-mixing technique for high-power single-cycle pulse synthesis in the visible and ultraviolet ranges," *Phys. Rev. A*, vol. 79, 063838, 2009.

[24] J. Liu and T. Kobayashia, "Cascaded four-wave mixing in transparent bulk media," *Opt. Commun*., vol. 283, pp. 1114–1123, 2009.

[25] J. Liu and T. Kobayashia, "Cascaded four-wave mixing and multicolored arrays generation in a sapphire plate by using two crossing beams of femtosecond laser," *Opt. Exp*., vol. 16, pp. 22119–22125, 2008.

[26] N. Forget, V. Crozatier, and T. Oksenhendler, "Pulse-measurement techniques using a single amplitude and phase spectral shaper," *J. Opt. Soc. Amer. B*, vol. 27, pp. 742–756, 2010.

[27] D. Keusters, H. Tan, P. OŚhea, E. Zeek, R. Trebino, and W. S. Warren, "Relative-phase ambiguities in measurements of ultrashort pulses with well-separated multiple frequency components," *J. Opt. Soc. Amer. B*, vol. 20, pp. 2226–2237, 2003.
[28] T. W. Hänsch, "A proposed sub-femtosecond pulse synthesizer using separate phase-locked lser oscillators," *Opt. Commun.*, vol. 80, pp. 71–75, 1990.
[29] W. Chen, Z. Hsieh, S. W. Huang, H. Su, C. Lai, T. Tang, C. Lin, C. Lee, R. Pan, C. Pan, and A. H. Kung, "Sub-single-cycle optical pulse train with constant carrier envelope phase," *Phys. Rev. Lett.*, vol. 100, p. 163906, 2008.
[30] M. Zhi, K Wang, X. Hua, and A. V. Sokolov, "Pulse-shaper-assisted phase control of a broadband coherent Raman spectral comb," unpublished.

Miaochan Zhi was born on August 16, 1975 in Luoyang, Henan Province, China. She received the B.E. degree in optical technology and photoelectric instrument, in 1996, and M.S. degree in optical physics, in 2001, from Zhejiang University, China. She joined Alexei Sokolov's Subfemtosecond Science Lab at Texas A&M University, in 2001, where she received a Ph.D. degree in ultrafast optics, in December 2007.

The year after receiving the Ph.D. degree, she worked for a private company investigating noninvasive glucose detection using femtosecond laser spectroscopy. Presently she works as a postdoctoral research associate with Prof. Alexei Sokolov on single-cycle pulse generation in Raman-active crystals. Her research interests include ultrashort pulse generation, nonlinear spectroscopy, and ultrafast laser application in biomedical research.

Dr. Zhi is a member of the Optical Society of America.

Alexei V. Sokolov was born on April 14, 1971, in Odessa, Ukraine, to a family of engineers. He received the first degree in physics, in 1994, from Moscow Institute of Physics and Technology, Moscow, Russia. In his diploma work, performed in Laser Biophysics Laboratory at the General Physics Institute, Russian Academy of Sciences, Moscow, he focused on the development of integrated optics sensors that use Langmuir-Blodgett films as sensing elements. In 2001, he received the Ph.D. degree in physics from Stanford University, Stanford, CA, where he worked in Edward L. Ginzton Laboratory under supervision of Steve Harris.

While in Harris's group at Stanford, he investigated electromagnetically induced transparency (EIT) effects in molecular systems, which lead to collinear generation of a wide coherent Raman spectrum with a possibility of subfemtosecond pulse compression. Later, he moved to Texas A&M University, TX, where he currently holds a professor position in physics and astronomy, and a Stephen E. Harris professorship in quantum optics. His overall expertise is in the field of laser physics, nonlinear optics, ultrafast science, and spectroscopy. His research interests center around applications of molecular coherence to quantum optics, ultrafast laser science and technology, including generation of subcycle optical pulses with prescribed temporal shape and their application to studies of ultrafast atomic, molecular, and nuclear processes, as well as applications in biological and defense-oriented areas. He maintains a well-funded group and has supervised a number of postdocs and graduate students who have won numerous student awards.

Prof. Sokolov is an elected Fellow of the Optical Society of America (OSA, 2009) and a member of the American Physical Society (APS). Some distinguished awards he received, include Adolph Lomb Medal (OSA, 2003), Research Innovation Award (Research Corporation, 2003), Montague Scholarship for Teaching Excellence (Texas A&M University, 2005), and Robert S. Hyer Award (Texas Section APS, 2007).